



# MOFs based on ZIF-8 deposited on TiO<sub>2</sub> nanotubes increase the surface adsorption of CO<sub>2</sub> and its photoelectrocatalytic reduction to alcohols in aqueous media



J.C. Cardoso<sup>a,\*</sup>, S. Stulp<sup>b</sup>, J.F. de Brito<sup>a</sup>, J.B.S. Flor<sup>a</sup>, R.C.G. Frem<sup>a</sup>, M.V.B. Zanoni<sup>a</sup>

<sup>a</sup> São Paulo State University (UNESP), Institute of Chemistry, Araraquara, Brazil

<sup>b</sup> Universidade do Vale do Taquari (UNIVATES), Center of Sciences and Engineering, Lajeado, Brazil

## ARTICLE INFO

### Keywords:

Metal Organic Frameworks  
Zeolite imidazole framework-8  
Methanol  
Ethanol  
Photoelectrocatalysis

## ABSTRACT

This work describes the decoration of Ti/TiO<sub>2</sub> nanotubes by nanoparticles of ZIF-8 (zeolite imidazole framework-8) grown using a layer-by-layer process. Morphological and crystallographic analyses showed that the TiO<sub>2</sub> nanotubes were coated with ZIF-8 nanoparticles around 50 nm in size. Curves of  $I_{ph}$  vs.  $E$  showed that the incorporation of ZIF-8 at Ti/TiO<sub>2</sub> electrodes increased the photocurrent and that the values were dramatically increased in solution saturated with CO<sub>2</sub>. The CO<sub>2</sub> adsorbed on the ZIF-8 formed stable carbamates, as demonstrated by spectroscopic and voltammetric assays. Photoelectrocatalytic reduction of CO<sub>2</sub> at Ti/TiO<sub>2</sub>NT-ZIF-8 electrodes resulted in formation of up to 10 mmol L<sup>-1</sup> of ethanol and 0.7 mmol L<sup>-1</sup> of methanol in 0.1 mol L<sup>-1</sup> Na<sub>2</sub>SO<sub>4</sub>, at  $E_{app}$  of +0.1 V, under UV-vis irradiation at room temperature. Our findings open up new applications of metal-organic frameworks (MOFs) in photoelectrocatalysis for the highly efficient preconcentration and conversion of CO<sub>2</sub> in aqueous media at ambient temperature.

## 1. Introduction

Energy production has progressively become a major global concern due to the depletion of natural resources and the problem of global warming. Therefore, it is essential to develop renewable energy sources that are environmentally friendly and economically viable. The conversion of CO<sub>2</sub> to value-added fuels or chemical products by direct use of sunlight is one of the most attractive processes, but ensuring selectivity remains a challenge [1–3].

CO<sub>2</sub> photoreduction involves multi-electron processes that can lead to a wide variety of products ranging from CO and CH<sub>4</sub> to higher hydrocarbons in the gas phase, and various oxygenates such as alcohols, aldehydes, and carboxylic acids in the liquid phase [1]. Consequently, there is increasing interest in the development of new catalytic materials that can increase performance for the conversion of CO<sub>2</sub> into these compounds. Metal-organic frameworks (MOFs) have been applied as an excellent alternative for the storage of fuels (hydrogen and methane) [4], the capture and preconcentration of carbon dioxide [5], and several applications in catalysis [6]. According to the official IUPAC definition, MOFs are coordination polymers with an open framework containing potential voids [7]. Members of this special class of coordination compounds are formed by the self-assembly of secondary

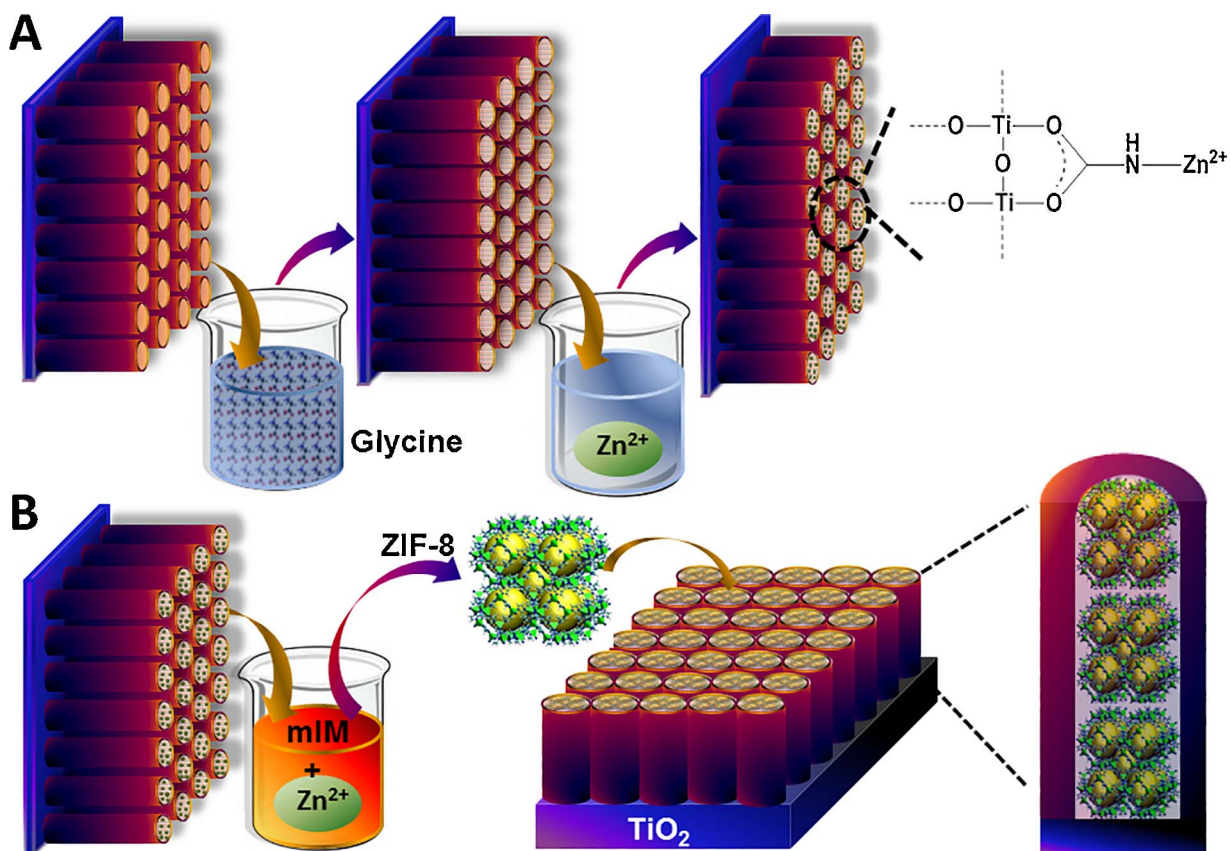
building units (SBUs) linked by strong metal-ligand covalent bonds, leading to the formation of infinite 3D networks with channels and cavities of regular size and shape [8,9]. They present permanent porosity, well-defined crystalline structure, very high surface area, and low density, and offer the possibility of functionalization of their pores [10]. Due to these properties, MOFs have shown promise for applications in areas including the storage and separation of gases [4,5,11], catalysis [6,12], chemical sensing [13], and biomedicine [8], among others [6].

In addition to carboxylate-based MOF materials, nonlinear N-based ditopic linkers can also be used for the construction of these types of porous coordination solids. A very important subclass of MOFs, the zeolitic imidazolate frameworks (ZIFs), has attracted interest mainly because these materials combine the advantages of the MOFs with the very high chemical and thermal stabilities of zeolites [14]. They are constructed from the coordination of tetrahedral divalent cations (Zn<sup>2+</sup>, Co<sup>2+</sup>, and Cd<sup>2+</sup>) with imidazole spacer ligands, whose frameworks resemble those of the zeolites. The Si-O-Si bond angle (145°) in silicate-based zeolites is close to the angle formed by imidazolates when bridging metal ions [15]. These robust materials have promising potential for use in a variety of practical applications, especially gas storage and separation [16] and catalysis [17].

The zinc-based compound [Zn(mIM)<sub>2</sub>], where mIM = 2-

\* Corresponding author.

E-mail address: [jcarvalho82@gmail.com](mailto:jcarvalho82@gmail.com) (J.C. Cardoso).

Fig. 1. ZIF-8 formation on Ti/TiO<sub>2</sub>NT.

methylimidazole, denoted ZIF-8 [18], has been successfully used for CO<sub>2</sub> greenhouse gas adsorption, due to its excellent stability, very high surface area (1881 m<sup>2</sup> g<sup>-1</sup>), and ease of synthesis, combined with highly selective CO<sub>2</sub> capture [19]. Since the aperture in ZIF-8 (with SOD topology) connecting large cavities (~1.5 nm) has a size of 0.34 nm, which is in the same range as the nominal kinetic diameter of CO<sub>2</sub> (0.33 nm), the known structural flexibility of this material is crucial for diffusion of the gas [12].

Therefore, given that ZIF-8 has been used for dioxide carbon capture, the present work investigates the integration of this very porous material with TiO<sub>2</sub> nanotubes in order to not only improve CO<sub>2</sub> uptake and activation (due to the basic sites on the imidazolate linkers), but also to improve catalyst efficiency in CO<sub>2</sub> transformation reactions. Recent studies have reported the use of some MOFs as co-catalysts in CO<sub>2</sub> photoreduction systems, in order to promote the transport of photoexcited electrons [20–24].

Photoelectrocatalysis is a technique that uses a semiconductor, such as TiO<sub>2</sub>, which under irradiation higher than the band gap energy is capable of generating e<sup>-</sup>/h<sup>+</sup> pairs that can be separated by means of a potential gradient established at the interface of the electrode (semiconductor) and the electrolyte [13,20–28]. The photoelectrocatalysis technique offers great versatility for use in the reduction of CO<sub>2</sub> to hydrocarbons with short and long carbon chains [32]. The electrons driven to the photocatalyst surface in a photoelectrocatalytic process [33] play a major role in the conversion of CO<sub>2</sub> to fuels or other chemical products. This is an attractive process, although remaining challenges include low dissolution of CO<sub>2</sub> in aqueous media and poor selectivity of the CO<sub>2</sub> reduction reaction [24,25,29–31,34–36].

In this context, Metal Organic Frameworks are used as a catalyst in systems for CO<sub>2</sub> conversion [37,38]. Some authors [24,39,40] have indicated that MOFs over graphitic carbon nitride nanotubes can convert CO<sub>2</sub> to a large variety of products, such as methane, methanol, formate, carbon monoxide by the photocatalysis, for instance.

Furthermore, in recent years Metal Organic Frameworks has been investigated in the electrochemical reduction of CO<sub>2</sub> [41–44], reaching different types of interesting products (formate, carbon monoxide, etc.). But, the use of MOFs in photoelectrocatalytic systems is scarce and the use of Ti/TiO<sub>2</sub> nanotubes as platforms for the deposition of thin films of catalytic ZIF-8 material seems an alternative for novel catalytic applications in the field of CO<sub>2</sub> conversion.

The development of Ti/TiO<sub>2</sub> nanotubes as platforms for the deposition of thin films of catalytic ZIF-8 material could lead to a variety of novel catalytic applications in the field of photoelectrocatalysis [45]. The use of this technique to reduce CO<sub>2</sub> is considered as the first report in the literature using this catalytic system. The present work reports, a new hybrid photocatalyst produced by growing thin films of ZIF-8 on Ti/TiO<sub>2</sub> nanotube electrodes. The aim was to develop a system able to increase CO<sub>2</sub> gas capture, with improved photoelectrocatalytic reduction to a fuel such as methanol. ZIF-8 was selected for this purpose due to its high surface area, excellent thermal and chemical stability, high capacity for the chemisorption and activation of CO<sub>2</sub> [20], and ability to mediate the reduction of CO<sub>2</sub> under UV irradiation at low applied potential. This work demonstrates that photoelectrocatalysis using a MOF-based Ti/TiO<sub>2</sub> composite has promising potential applications in the fields of energy conversion and environmental protection.

## 2. Materials and methods

### 2.1. Formation of TiO<sub>2</sub> nanotube arrays

Organized self-assembled nanotubes of TiO<sub>2</sub> (TiO<sub>2</sub>NT) were obtained by anodizing clean 10 cm<sup>2</sup> titanium foil samples (Realum, Brazil) that were polished with silicon carbide sandpaper of different roughness (220, 320, 400, 800, 1200, and 1500 grit), sonicated for 15 min in isopropanol, acetone, and ultrapure water, and dried in a flow of N<sub>2</sub> [13]. Anodizing was performed by immersing the foils (at room

temperature) in glycerol/water (90:10 v/v) containing 0.25%  $\text{NH}_4\text{F}$  (Sigma-Aldrich), for 50 h, in an electrochemical cell. A voltage of 30 V was provided using a DC power supply (Minipa MPL-1303), and a Ti/Ru DSA<sup>®</sup> (De Nora) was used as the counter electrode. The samples were subsequently rinsed with deionized water, dried in a nitrogen stream, and annealed at 450 °C for 1 h in air, using a heating rate of 2 °C min<sup>-1</sup>.

## 2.2. Formation of ZIF-8 nanoparticleS ON $\text{TiO}_2$ nanotube arrays

Firstly, the Ti/TiO<sub>2</sub>NT electrode was immersed for 1 h in a 0.3 mol L<sup>-1</sup> aqueous glycine solution (Fig. 1), followed by washing with deionized water and drying at 50 °C for 2 h. After drying, the nanosstructured  $\text{TiO}_2$  material was immersed in a 0.1 mol L<sup>-1</sup> zinc(II) acetate solution for 20 min and then dried for 10 h at 50 °C. The reaction medium for formation of the MOF, using a metal:ligand molar ratio of 1:70, was prepared by weighing out 7.566 g (92.1 mmol) of 2-methylimidazole into a beaker and dissolving it in 26.66 mL of deionized water. The pretreated electrode was then immersed in this solution for 1 h, under stirring. Finally, a solution containing 0.390 g (1.3 mmol) of  $\text{Zn}(\text{NO}_3)_2 \cdot 6\text{H}_2\text{O}$  dissolved in 2.66 mL of deionized water was added, with stirring continued for 3 h.

## 2.3. Photoreactor

The stainless steel photochemical reactor (250 mL total volume, with 200 mL for solution and 50 mL for headspace) used in these experiments was constructed to maintain constant distances between the electrodes and the illumination source, hence ensuring the reproducibility of the measurements. The distance between each electrode was 1.0 cm, and a 20 cm<sup>2</sup> quartz window in the wall of the reactor was at a distance of 0.8 cm from the working electrode. The pressure of the system was controlled with a manometer. Gas and liquid samples were collected through a silicone septum, using a gastight syringe. The solution was stirred using a magnetic bar in the base of the reactor. All the measurements were made at a pressure of 1 atm. A schematic illustration of the reactor is provided in Fig. 2.

## 2.4. Photocatalytic and $\text{CO}_2$ reduction experiments

All the  $\text{CO}_2$  reduction experiments were performed for a period of 3 h, employing the following techniques: photoelectrocatalysis (PEC), photocatalysis (PC), photolysis (PT), and electrolysis (ET). The PEC experiments were conducted at controlled potential, using  $\text{TiO}_2$  nanotubes with and without ZIF-8 decoration as the working electrodes. The reference electrode was Ag/AgCl in 3.0 mol L<sup>-1</sup> KCl, and the counter

electrode was a DSA<sup>®</sup> plate. The working electrode was illuminated by UV-vis light using a 125 W mercury vapor lamp positioned at a 5.0 mm distance outside the reactor. The PC experiments used the same system, but only with the catalyst irradiated by UV-vis light. The PT and ET experiments used the same reactor system with and without UV-vis irradiation, respectively. Before each experiment, the 0.1 mol L<sup>-1</sup>  $\text{Na}_2\text{SO}_4$  supporting electrolyte was saturated by bubbling  $\text{CO}_2$  through the solution for 1 h, using a gas diffuser system to reduce the bubble size and improve the mass transfer of the gas. This solution was then added to the reactor, which was sealed to prevent loss of the gas. An approximately 50 mL headspace was provided for collection of the gaseous products generated in the catalytic reaction.

## 2.5. Identification and quantification of the products generated by $\text{CO}_2$ reduction

The products formed after  $\text{CO}_2$  reduction were identified and quantified by gas chromatography with flame ionization detection (GC-FID), using a Shimadzu model 2010 instrument. For analysis of liquid samples, extraction of the products was performed by transferring a 0.5 mL aliquot of the photoelectrolyzed solution to a sealed 1.5 mL container and heating in a bath for 7 min at 65 °C. After this time, a 75  $\mu\text{m}$  Carboxen/PDMS fiber (Supelco) was exposed to the vapors in the container for 5 min, followed by injection into the gas chromatograph. A Restec Stabilwax chromatographic column was used (30 m  $\times$  0.25 mm i.d.; 25  $\mu\text{m}$  film thickness). The carrier gas was nitrogen, at a flow rate of 1.0 mL min<sup>-1</sup>. The injector was operated in splitless mode at 250 °C, and the detector temperature was 260 °C. The column oven heating program was an initial temperature of 40 °C, followed by heating at 2 °C min<sup>-1</sup> up to 46 °C, and then at 45 °C min<sup>-1</sup> up to 170 °C, with the final temperature held for 3 min. Headspace analysis was performed by direct injection of aliquots collected with a gastight syringe. The concentrations of the products obtained in the SPME and headspace analyses were summed to give the total concentration of the products formed.

## 2.6. Characterization of THE photoelectrodes

Field emission gun scanning electron microscopy (FEG-SEM), using a JEOL 7500F microscope and Transmission electron microscopy (TEM) CM Super Twin 200 transmission electron microscope (TEM) (Philips/FEI, Eindhoven, Netherlands) operated at 200 kV. Samples were prepared by ultrasonically dispersing the catalyst into isopropyl alcohol, then placing a drop of this suspension onto a copper grid, were employed to analyze the morphologies of the tubular  $\text{TiO}_2$  nanostructures, with and without decoration with ZIF-8 nanoparticles. The crystallinities of the synthesized materials were evaluated by X-ray diffraction (XRD), using a Siemens D5000 diffractometer with Cu-K $\alpha$  radiation, controlled by DIFFRACplus XRD Commander software. The X-ray photoemission spectra was obtained with a Scienta Omicron ESCA + spectrometer system equipped with a E A125 hemispherical analyzer and a X m 1000 monochromated x-ray source in Al k  $\alpha$  (1486.7 eV). It was used a Cn10 Omicron Charge neutralizer with an beam energy in 1.6 eV for charge effects compensation. The binding energy were calibrated using C 1s peak at 284.8 eV. Fourier transform infrared spectroscopy (FTIR) spectra were obtained using a Diamond ATR (attenuated total reflectance) accessory and a Bruker Vertex 70 spectrometer equipped with a DLaTGS detector, in the range 4000–400 cm<sup>-1</sup>. DRIFTS (diffuse reflectance infrared Fourier transform spectroscopy) experiments were performed using the same equipment with an EasyDiff accessory (Pike Technology, Madison, WI, USA). In order to evaluate the interaction between carbon dioxide and the materials, samples of activated ZIF-8 and Ti/TiO<sub>2</sub>-ZIF-8 composite were prepared for the FTIR-ATR and DRIFTS measurements by pressurizing the reaction chambers (illustrated in Figs. S1 and S2, respectively) for 24 h with  $\sim$  5 atm of  $\text{CO}_2$ . Evaluation of the photoactivity and Mott-Schoktt plot

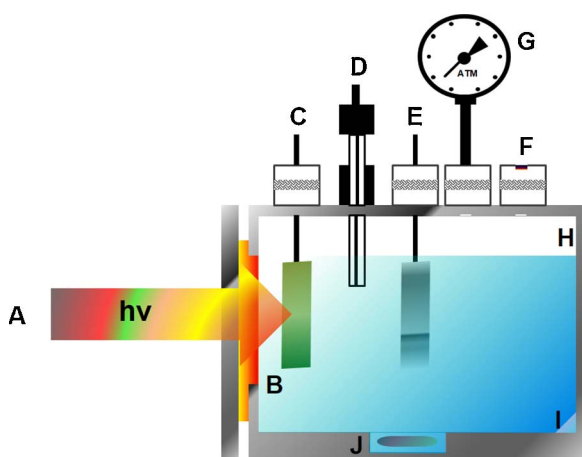


Fig. 2. Photoreactor used in all the experiments. (A) 125 W mercury vapor lamp; (B) quartz window; (C) working electrode; (D) reference electrode; (E) counter electrode; (F) septum; (G) manometer; (H) headspace; (I) supporting electrolyte; (J) magnetic bar.

of the electrodes and the photoelectrolysis employed an Autolab PGSTAT model 302 potentiostat/galvanostat, controlled using NOVA 1.10 software. The photocurrent was measured by linear scanning voltammetry, using the Ti/TiO<sub>2</sub>NT with and without ZIF-8 nanoparticles as the working electrode, Ag/AgCl in 3.0 mol L<sup>-1</sup> KCl as the reference electrode, and a D e Nora DSA<sup>®</sup> as the counter electrode, in an electrolyte of 0.1 mol L<sup>-1</sup> Na<sub>2</sub>SO<sub>4</sub> (pH 6.8). The scan rate used was 10 mV s<sup>-1</sup>. Mott-Schottky plots were analyzed using the impedance-potential mode in darkness at a fixed frequency of 3.0 Hz at potential ranged from -0.8 to 1.0 V vs Ag/AgCl in KCl 3 mol L<sup>-1</sup> and scan rate 50 mV s<sup>-1</sup>. For CO<sub>2</sub> reduction, the electrochemical system was operated at constant potentials of -0.7 V and 0.1 V for 3 h. An Agilent Cary 60 UV-vis spectrophotometer was used to measure the absorption and diffuse reflectance spectra of the materials and to calculate the band gap of the catalyst.

Tauc graphs were used to estimate the band gap energies of the materials. This method consists of extrapolating the linear portion of a plot of  $\alpha(hv)^{1/\gamma}$  as a function of  $hv$  (eV), where the intercept at  $\alpha = 0$  is the optical band gap ( $E_{bg}$ , in eV). In these expressions,  $\alpha$  is the absorption coefficient,  $h$  is Planck's constant (J s),  $v$  is the frequency (s<sup>-1</sup>), and  $\gamma$  is the power coefficient, whose values can be 1/2, 3/2, 2, or 3, depending on the type of electronic transition: direct allowed, direct forbidden, indirect allowed, and indirect forbidden, respectively. The diffuse reflectance measurements were converted to equivalent absorption coefficients using the Kubelka-Munk (K-M) method.

### 3. Results and discussion

#### 3.1. FEG-SEM and tem analysis

Fig. 3A–C show scanning electron microscopy images of TiO<sub>2</sub> nanotubes before and after coating with ZIF-8 by means of the layer-by-layer deposition process. The bare TiO<sub>2</sub>NT electrode (Fig. 3A) showed the formation of tubes with diameters changing from 90 to 100 nm, thickness of from 20 to 30 nm, and length around 1.2  $\mu$ m [21,33]. The incorporation of ZIF-8 on the TiO<sub>2</sub> nanotubes (Fig. 3B and C) resulted in

agglomerates of nanoparticles formed by nucleation and growth, with an average size of 50–57 nm, distributed over the entire surface of the TiO<sub>2</sub> nanotubes, without complete blocking of the nanotubes by ZIF-8 molecules. Fig. 3D shows energy dispersive X-ray spectra for the same electrode. The EDS spectrum (Fig. 3D) revealed the presence of Ti, C, N, O and Zn related to the metal-organic complex synthesized on the Ti/TiO<sub>2</sub>NT-ZIF-8 electrode. Fig. 3E–F shows the images obtained by TEM for Ti/TiO<sub>2</sub>NT and Ti/TiO<sub>2</sub>NT-ZIF-8, respectively, and it is possible to observe the presence of these ZIF-8 nanoparticles between and within the TiO<sub>2</sub> nanotubes.

The energy-dispersive X-ray spectroscopy (EDS) elemental mapping performed for the Ti/TiO<sub>2</sub>NT-ZIF-8 catalyst is shown in Fig. 4. The presence of the Zn element uniformly throughout the analyzed sample is observed along with the other expected elements such as C, N, O and Ti.

#### 3.2. XRD analysis

Powder X-ray diffractograms of simulated and synthesized ZIF-8 crystals are shown in Fig. 5, with the matching curves indicating formation of the ZIF-8 phase. The experimental ZIF-8 spectrum (Fig. 5B) exhibited sharp peaks, in excellent agreement with the simulated spectrum obtained using Mercurial software (Fig. 5A). The spectrum for a ZIF-8 single crystal, available from the Cambridge Crystallographic Data Centre database (file CCDC 602542), confirmed the crystallinity of the synthesized samples consisting of nano-sized crystals with nearly rhombic dodecahedron shapes [10,14]. Average sizes of these particles of between 50 and 57 nm were calculated using the Scherrer equation, in agreement with the values obtained from the FEG-SEM images.

#### 3.3. X-ray photoelectron spectroscopy

Fig. 6A–F shows the spectra using the XPS technique to evaluate the composition and chemical states of Ti/TiO<sub>2</sub>NT-ZIF-8 catalyst. A broad spectrum analyzed (Fig. 6 (Curve A) shows the prominent presence of the main peaks expected for this material. The high resolution XPS

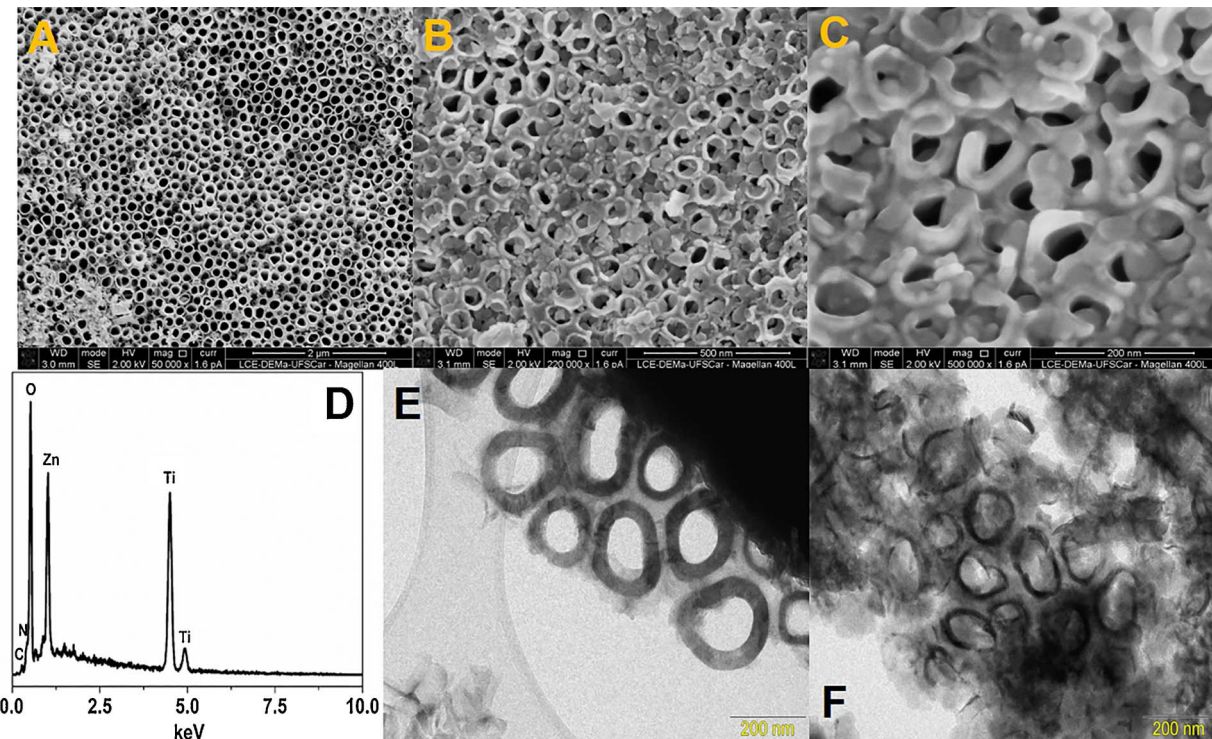


Fig. 3. Morphological characterization of ZIF-8 nanoparticles incorporated on TiO<sub>2</sub> nanotubes. A: FEG/SEM image of pure TiO<sub>2</sub> nanotubes; B and C: FEG/SEM images of nanoparticles of ZIF-8 incorporated on Ti/TiO<sub>2</sub>NT, at two different magnifications; D SEM-EDS spectrum of Ti/TiO<sub>2</sub>NT-ZIF-8; E: TEM of Ti/TiO<sub>2</sub> nanotube and (F) TEM of Ti/TiO<sub>2</sub>NT-ZIF-8.

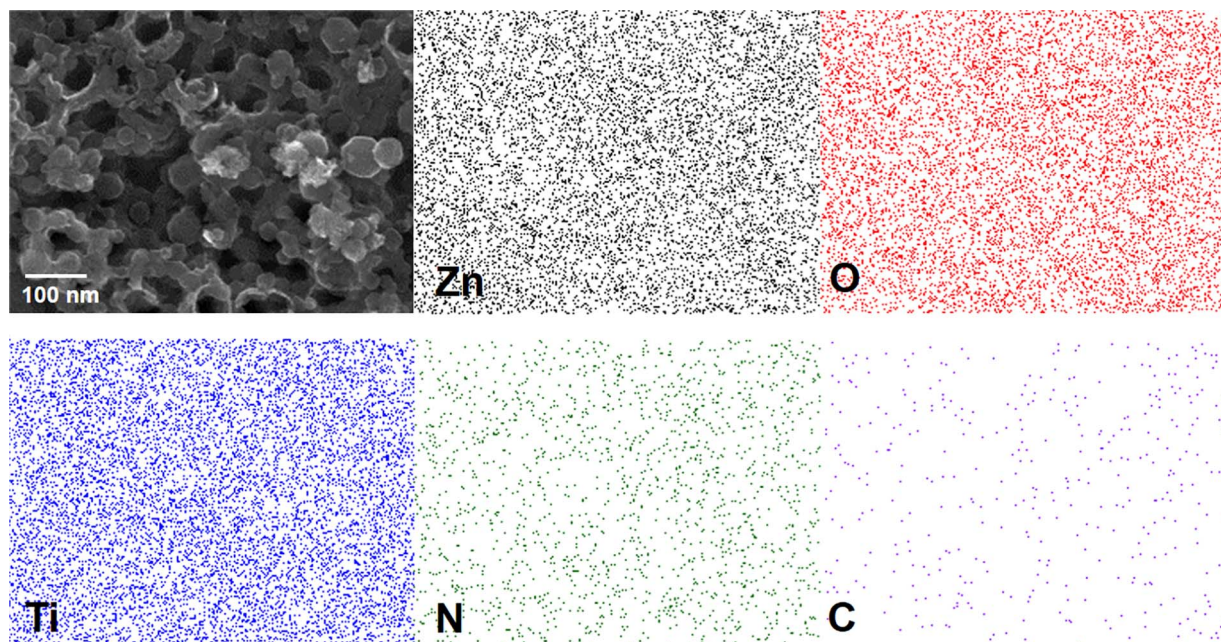
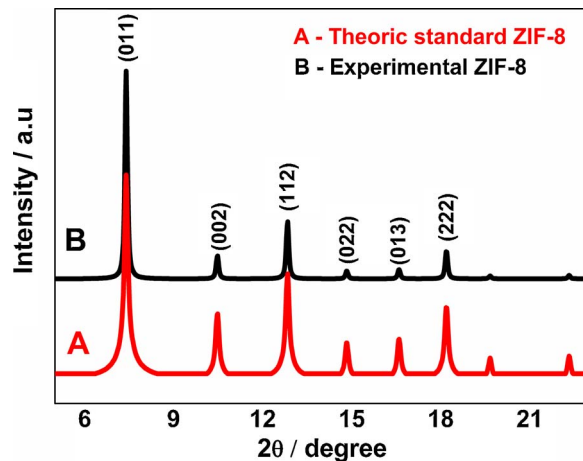
Fig. 4. EDX elemental mapping of Ti/TiO<sub>2</sub>NT-ZIF-8.

Fig. 5. XRD diffractograms of ZIF-8: (A) simulated; (B) experimental.

spectra for each element analyzed is shown by Fig. 6(Curves B–F) to: Zn 2p; Ti 2p; N 1s; O 1s and C 1s, respectively. According to these analyzes the presence of the main elements in their respective states were observed as shown in each individual spectrum and when compared with similar values presented in the literature, present a very significant similarity. The Ti 2p and O 1s peaks for TiO<sub>2</sub> nanotubes indicate that there is no complete coating of the entire surface by the ZIF-8 nanoparticles [46–48].

#### 3.4. UV-vis analysis

The absorption spectra of the synthesized materials are shown in Fig. 7A. The spectrum for ZIF-8 (black curve) showed no absorption in the visible region, while bands in the UV region, at 225 and 307 nm, could be attributed to absorption of the 2-methylimidazole linker. From comparison of the spectra for Ti/TiO<sub>2</sub>NT and Ti/TiO<sub>2</sub>NT-ZIF-8, it can be seen that the absorption increased for the latter, indicative of effective interaction between the TiO<sub>2</sub> nanotubes and the ZIF-8 nanoparticles and consequent diversification of the options for photoelectrode activation. Calculations using the Kubelka-Munk equation indicated that the addition of ZIF-8 resulted in a shift of the band gap potential from

3.2 to 2.8 eV as shown in Fig. 7B.

#### 3.5. Infrared spectroscopy

FTIR-ATR and DRIFTS experiments were carried out in order to investigate CO<sub>2</sub> capture by ZIF-8. Fig. S3 shows FTIR-ATR spectra of the activated MOF before (red) and after (black) CO<sub>2</sub> exposure. The main vibrational modes of the carbon dioxide molecule, associated with the  $\nu_{as}C=O$   $\nu_3$ ,  $\nu_1$ , and  $\nu_2$  bending bands, are found in the gas phase CO<sub>2</sub> spectrum at 2349, 1388, and 667 cm<sup>-1</sup>, respectively [49], as can be observed in Fig. S3 (see also Table S1). The spectrum obtained for ZIF-8 after exposure to the carbon dioxide atmosphere showed the corresponding bands at 2339/2360, 1382, and 672 cm<sup>-1</sup>, in addition to typical CO<sub>2</sub> combination bands ( $\nu_3 + \nu_1$  and  $\nu_3 + 2\nu_2$ ) near 3700 and 3600 cm<sup>-1</sup>, respectively. The presence of two bands in the C=O antisymmetric stretching region (at 2339 and 2360 cm<sup>-1</sup>) could be explained by the presence of two distinct CO<sub>2</sub> interaction sites (see the DRIFTS results). The characteristic FTIR-ATR bands of ZIF-8 are also provided in Table S1 [50].

The adsorption of CO<sub>2</sub> was confirmed by DRIFTS spectroscopy, which is an important tool for obtaining information about the nature of the interactions between the adsorbed CO<sub>2</sub> molecules and the framework [51]. The DRIFTS spectra of the framework before and after loading using 5 atm of CO<sub>2</sub> showed evidence of host-guest interactions (Fig. 8). CO<sub>2</sub> is a linear molecule with high polarizability, and after interaction with the MOF, the corresponding band assigned to the  $\nu_3$  vibrational mode (at 2349 cm<sup>-1</sup>) was shifted to 2360 cm<sup>-1</sup>. Satellite peaks at 2367/2354 and 2365/2357 cm<sup>-1</sup> in the DRIFTS spectrum revealed the presence of more than one interaction site. It has been reported that in addition to the adsorption of carbon dioxide guest molecules in the pores of ZIF-8 (where the diameter of the hexagonal channels is around 0.34 nm) [52], the organic linkers also provide important CO<sub>2</sub> interaction sites [53]. The spectroscopic results obtained here were consistent with the previous findings, since an absorption band at around 1600 cm<sup>-1</sup> in the spectrum of ZIF-8 loaded with the gas (see Fig. S3) was assigned to the C=C stretching mode of the imidazole ring and was not present in the spectrum for the empty framework. This observation confirmed the interaction between CO<sub>2</sub> and the MOF at the specific site of the imidazole linker. There was also evidence of the formation of carbamate species from the interaction between CO<sub>2</sub> and

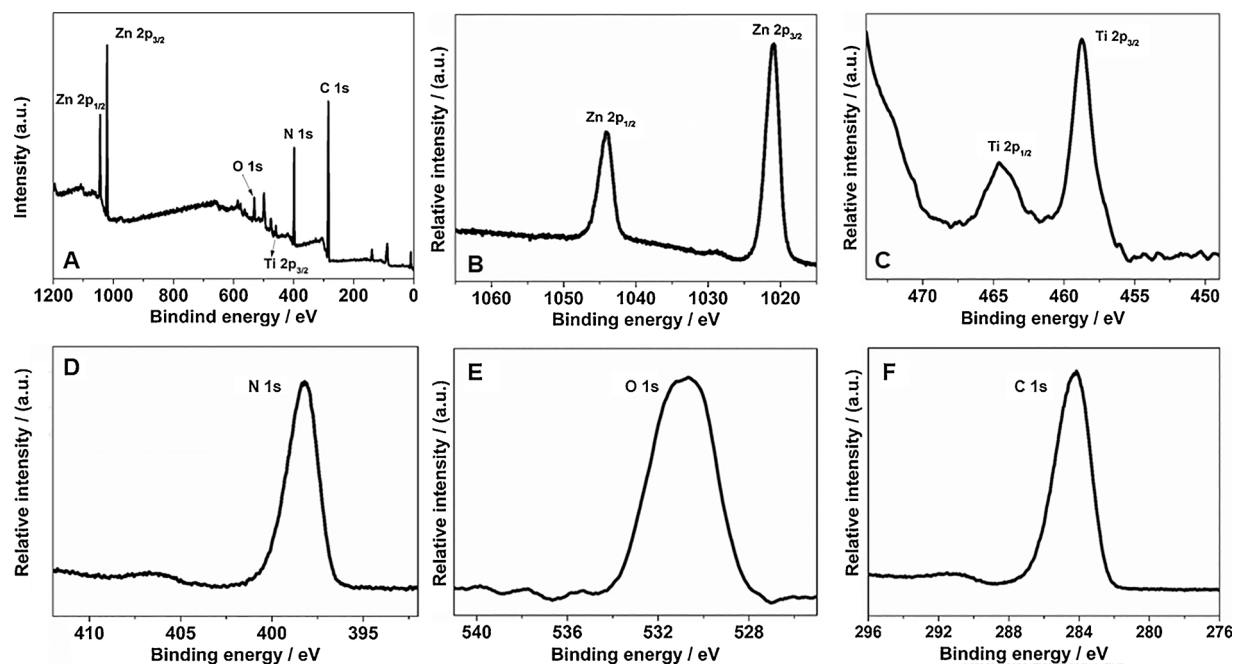


Fig. 6. XPS survey spectra of the sample Ti/TiO<sub>2</sub>NT-ZIF-8 (A) and the corresponding high resolution XPS spectra of: (B) Zn 2p; (C) Ti 2p; (D) N 1s; (E) O 1s and (F) C 1s.

2-methylimidazole molecules at the surfaces of the ZIF-8 particles [54]. For example, the presence of a band at 1334 cm<sup>-1</sup> in the FTIR-ATR spectra for CO<sub>2</sub> adsorbed onto the ZIF-8 and ZIF-8/TiO<sub>2</sub>NT materials (see Table S1) was in good agreement with the value reported by Long et al. [55] and could be attributed to the C–N vibrational mode of carbamate species.

Based on the high CO<sub>2</sub> capture capacity of the ZIF-8 [19] and DRIFTS spectroscopic results, it can be suggested that there still seems to be a significant interaction between CO<sub>2</sub> molecules and the ZIF-8/TiO<sub>2</sub> NT composite. The comparative analysis between the FTIR-ATR spectra shown in Fig. S4 once again confirms the successful growth of ZIF-8 on the TiO<sub>2</sub> nanotubes. Furthermore, the spectrum for CO<sub>2</sub> adsorbed on the ZIF-8/TiO<sub>2</sub>NT composite also showed the C–N band characteristic of the formation of carbamate species (at 1334 cm<sup>-1</sup>) (Fig. S4).

### 3.6. Photoactivity and electronical properties of the electrodes

The behaviors of the curves of the photocurrent plotted against potential obtained for the Ti/TiO<sub>2</sub>NT electrode in 0.1 mol L<sup>-1</sup> Na<sub>2</sub>SO<sub>4</sub> were compared with those for Ti/TiO<sub>2</sub>NT-ZIF-8 in 0.1 mol L<sup>-1</sup> Na<sub>2</sub>SO<sub>4</sub> in the presence and absence of saturated CO<sub>2</sub> in the electrolyte (Fig. 9X) while Fig. 9Y shows Mott-Schottky plots examined by the same electrodes.

Since Ti/TiO<sub>2</sub>NT is an n-type semiconductor, electron-hole pairs are

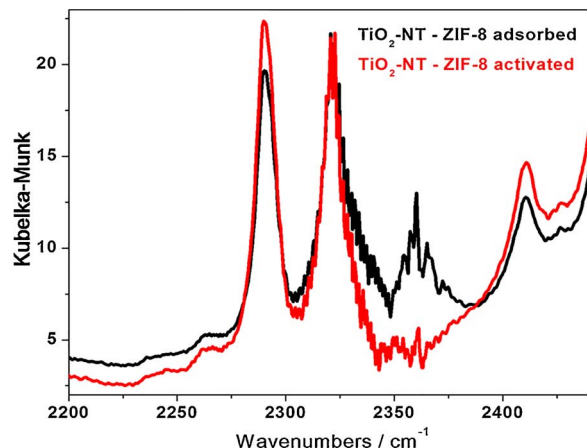


Fig. 8. DRIFTS spectra of ZIF-8 before (red) and after (black) exposure to CO<sub>2</sub>, acquired at ambient temperature. The spectra are plotted in Kubelka-Munk units. (For interpretation of the references to colour in this figure legend, the reader is referred to the web version of this article.)

only generated at the electrode surface when it is irradiated by light with energy greater than that of the band gap ( $\lambda < 380$  nm). Curve 9X (A) shows the behavior of the electrodes in the dark, with no charge carriers being generated during the potential scan, as expected. A bias

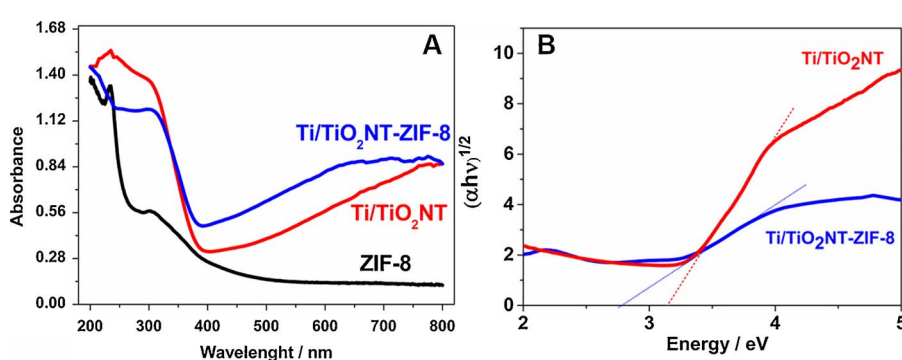
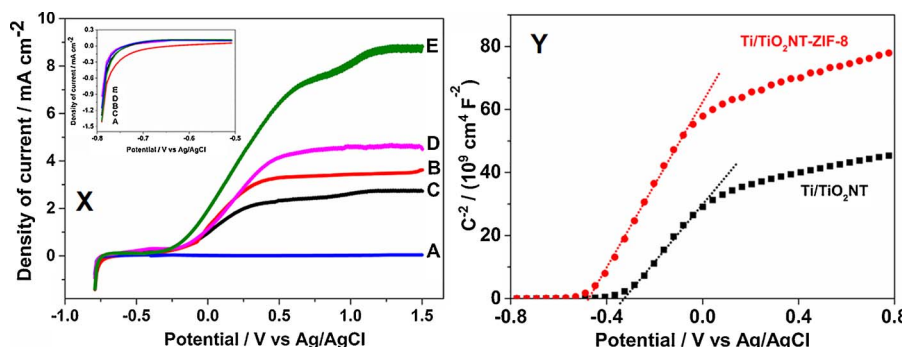
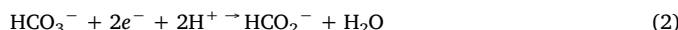


Fig. 7. UV-vis absorption spectra of ZIF-8, TiO<sub>2</sub>NT, and TiO<sub>2</sub>NT-ZIF-8 (A) and Tauc plot of Ti/TiO<sub>2</sub>NT and Ti/TiO<sub>2</sub>NT-ZIF-8 (B).



potential more positive than the flat band potential produces a bending of the conduction band, causing greater charge separation ( $e^-/h^+$ ), with holes being driven to the electrode surface. This generates hydroxyl radicals from water oxidation at  $E > E_{fb}$  [33]. The  $E_{fb}$  (flat band potential) for Ti/TiO<sub>2</sub> under these conditions is around  $-0.35$  V vs. Ag/AgCl [56–60], therefore there are an increasing of the photocurrent (curve B). But the photocurrent increased by 33% for Ti/TiO<sub>2</sub>NT-ZIF-8 (curve D), and at negative bias potential there is no significant change in the photocurrent, showing that there was ineffective charge separation (shown in the insert of Fig. 9X) for both electrodes. These results showed that ZIF-8 could act as an electron trap, improving separation of the charge carriers [57].

In the presence of CO<sub>2</sub>, there was a decrease of 25% in the photocurrent for Ti/TiO<sub>2</sub> (curve C), which could be attributed mainly to equilibrium processes of CO<sub>2</sub> in aqueous solution (Eqs. (1) and (2)). It is known that the presence of acid carbonate in solution can trap photo-generated electrons and decrease the separation of charges formed during the process [42–44].



The effect of CO<sub>2</sub> on the Ti/TiO<sub>2</sub>NT-ZIF-8 is shown in Fig. 9X (curves D and E). The photocurrent increased by 97% when the modified electrode was used in 0.1 mol L<sup>-1</sup> Na<sub>2</sub>SO<sub>4</sub> saturated with CO<sub>2</sub>. This suggested that the effective interaction of CO<sub>2</sub> with the ZIF-8 nanoparticles incorporated into the TiO<sub>2</sub>NT increased CO<sub>2</sub> capture in the selective MOF, as demonstrated in the DRIFTS experiments. The high efficiency of capture of CO<sub>2</sub> molecules could be attributed to the formation of carbamate compounds, as shown in Scheme 1 [16]. Vimont et al. [61] proposed that this reaction can lead to the formation of similar complexes for a class of structures containing reduced nitrogenated sites of imidazolate groups. Imidazole compounds can act as electron acceptors, and in a system containing Ti/TiO<sub>2</sub> activated by UV-vis irradiation, they could behave as mediators of electron donation, as well as improve the absorption of UV-vis radiation (Fig. 7). Therefore, the greater number of electrons photogenerated from this interaction dramatically increased the photocurrent. Hence, the CO<sub>2</sub> dissolved in the supporting electrolyte could adsorb strongly onto the ZIF-8 complex, due to the presence of the nitrogenated sites of the imidazolate groups, forming carbamates that could be reduced during the photoelectrocatalysis.

The IR spectroscopy results (Fig. 8) provided further evidence of carbamate formation when CO<sub>2</sub> was mainly preconcentrated on the ZIF-8 surface. A similar finding was reported by McDonald et al. [15] for a MOF with nitrogenous clusters. Knofel et al. [16] used infrared spectroscopy to investigate nitrogenous modifying groups and reported the formation of carbamylc compounds as major products. All these studies highlighted the greater effectiveness of interaction of CO<sub>2</sub> with nitrogen groups than with Ti cations or OH groups. Therefore, these species were more liable to be reduced by the electrons photogenerated on the surface of the Ti/TiO<sub>2</sub> catalyst decorated with ZIF-8, following

**Fig. 9.** (X) Linear scanning voltammograms of the electrodes: (A) both electrodes in the dark; (B) Ti/TiO<sub>2</sub>NT without CO<sub>2</sub>; (C) Ti/TiO<sub>2</sub>NT with CO<sub>2</sub>; (D) Ti/TiO<sub>2</sub>NT-ZIF-8 without CO<sub>2</sub>; (E) Ti/TiO<sub>2</sub>NT-ZIF-8 with CO<sub>2</sub>. Conditions:  $v = 10$  mV s<sup>-1</sup>; 0.1 mol L<sup>-1</sup> Na<sub>2</sub>SO<sub>4</sub>; pH 6.8 (without CO<sub>2</sub>); pH 4.5 (with CO<sub>2</sub>); illumination using a 125 W high pressure Hg vapor lamp and (Y) Mott-Schottky plot collected at 3.0 Hz for Ti/TiO<sub>2</sub>NT and Ti/TiO<sub>2</sub>NT-ZIF-8.

activation under UV-vis light and with an applied potential.

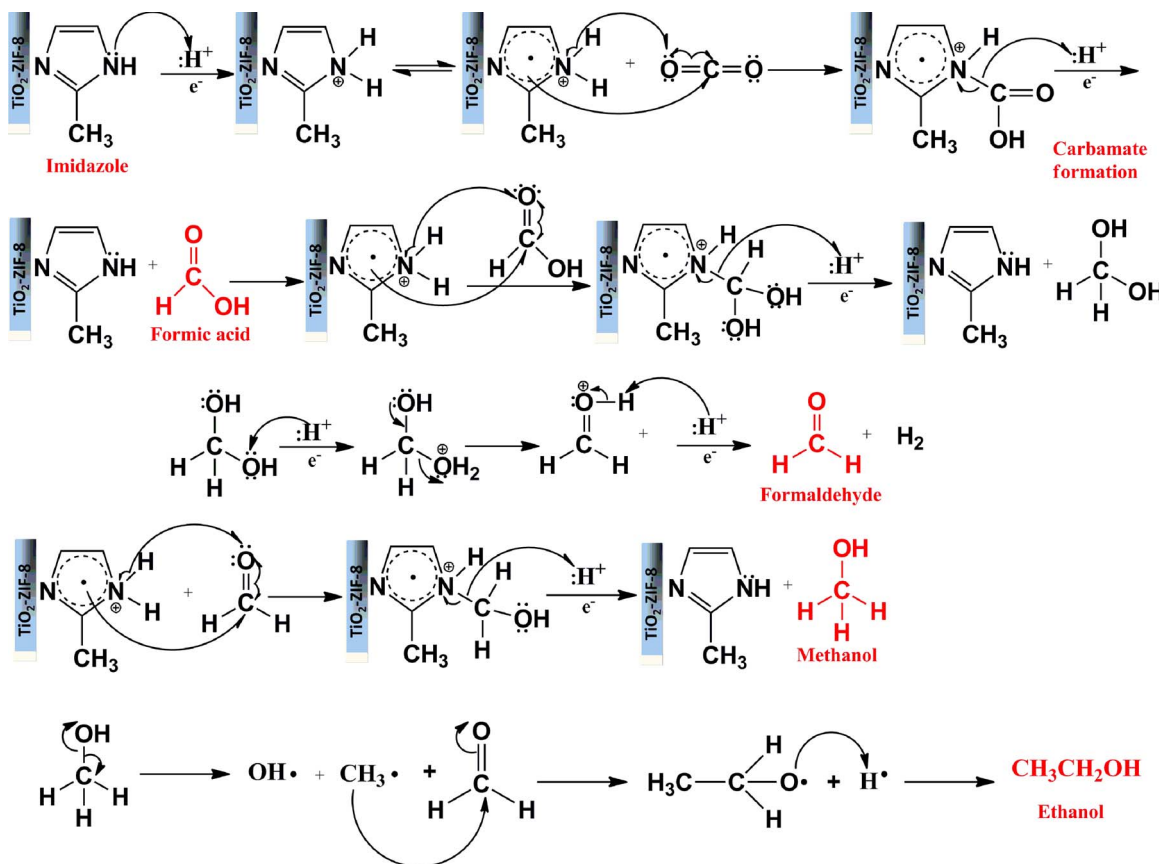
Mott-Schottky plots of the Ti/TiO<sub>2</sub>NT and Ti/TiO<sub>2</sub>NT-ZIF-8 electrodes were studied to evaluate the positioning of their respective electronic bands structures. As shown in Fig. 9Y, both curves showed positive slopes in Mott-Shottky plots at a frequency of 3.0 Hz, which is the typical n-type semiconductor behavior [48]. So, their flat band potentials are comparable to the conduction band potential. From the obtained curves it was possible to calculate the flat band potential of Ti/TiO<sub>2</sub>NT and Ti/TiO<sub>2</sub>NT-ZIF-8 at  $-0.35$  V and  $-0.50$  V versus Ag/AgCl at pH 6.8, respectively. Thus, combining the band gap values obtained from the optical analysis of each material (Fig. 7B) it was possible to estimate the position of the energy bands of the materials produced (Fig. S5). From these values it is highlighted that the potential of the conduction band is thermodynamically favorable to promote the reduction of CO<sub>2</sub> to several products, such as: CO<sub>2</sub>/CH<sub>4</sub>:  $-0.24$  V; CO<sub>2</sub>/CH<sub>3</sub>OH:  $-0.35$  V and CO<sub>2</sub>/CH<sub>3</sub>CH<sub>2</sub>OH:  $-0.33$  V versus Ag/AgCl pH 7.0 [62].

### 3.7. PhotoelectrocatalYTIC reduction of CO<sub>2</sub> at Ti/TiO<sub>2</sub>NT- ZIF-8

Firstly, the performance of the Ti/TiO<sub>2</sub>NT and Ti/TiO<sub>2</sub>NT-ZIF-8 electrodes was evaluated for reduction of CO<sub>2</sub> during 60 min of photoelectrocatalysis in 0.1 mol L<sup>-1</sup> Na<sub>2</sub>SO<sub>4</sub> (pH 4.5) saturated with CO<sub>2</sub>, under UV-vis irradiation and with an applied potential of  $-0.7$  V vs. Ag/AgCl. The main products formed in the process were methanol and ethanol (Fig. 10A and B). Other products such as acetone and formic acid were generated, but at very low concentrations that were below the quantification limits. The photoreduction of CO<sub>2</sub> to methanol and ethanol at the Ti/TiO<sub>2</sub>NT electrode was very low, this behavior can be attributed to the low capacity of Ti<sup>4+</sup> species to adsorb CO<sub>2</sub> in their structure, as described by Bhattacharyya et al. [63]. There was low CO<sub>2</sub> adsorption at the TiO<sub>2</sub> surface, and the Fermi energy level and formal potential of CO<sub>2</sub>/CH<sub>3</sub>OH were not sufficiently aligned for electron transfer [64]. The same performance of CO<sub>2</sub> reduction using the nanotubular TiO<sub>2</sub> electrodes were recorded evaluating the other conditions of analysis.

When the Ti/TiO<sub>2</sub>NT-ZIF-8 catalyst was used, the conversion of CO<sub>2</sub> to methanol and ethanol increased almost 20-fold and 430-fold, respectively (Fig. 10A), demonstrating the remarkable effect of the complex on the conversion of CO<sub>2</sub> to ethanol fuel. This could be explained by the efficient preconcentration of CO<sub>2</sub> on the electrode modified with ZIF-8 by interaction with the nitrogenated sites of the imidazolate groups in the ZIF-8 complex (Scheme 1), as confirmed by the IR spectroscopy analyses (Fig. 8). Fig. 10B illustrates the effect of photoelectrocatalysis times ranging from 0 to 3 h, using the Ti/TiO<sub>2</sub>NT-ZIF-8 electrode. The methanol concentration remained almost constant throughout the catalysis, while there was a substantial progressive increase of the ethanol concentration between 1 and 3 h of photoelectrocatalysis.

The influence of the bias potential applied in the photoelectrocatalytic system was evaluated using photoreduction at  $-0.7$  V and  $+0.1$  V vs. Ag/AgCl, under UV-vis irradiation. The results (Fig. 11)



**Scheme 1.** Proposed mechanism for alcohol formation using  $\text{Ti}/\text{TiO}_2\text{NT-ZIF-8}$  electrodes operated under UV-vis irradiation and with application of an external potential.

showed that the main products were methanol and ethanol, with a potential of  $+0.1\text{ V}$  providing 42.5% and 20% higher yields, respectively, which could be attributed to better separation of the electron/hole charges. The bending of the conduction bands was more effective at  $+0.1\text{ V}$ , favoring the transfer of photogenerated electrons towards the ZIF-8 on the surface of the electrode, where  $\text{CO}_2$  was pre-concentrated in the form of carbamyl compounds.

### 3.8. Comparison of photoelectrocatalysis, photocatalysis, photolysis, and electrolysis FOR $\text{CO}_2$ reduction at ZIF-8

In order to evaluate the relative importance of applied potential and UV-vis irradiation in the process of  $\text{CO}_2$  reduction to alcohols at  $\text{Ti}/\text{TiO}_2\text{NT-ZIF-8}$ , photoelectrocatalysis was carried out for 3 h in  $0.1\text{ mol L}^{-1}\text{ Na}_2\text{SO}_4$  (pH 4.5) saturated with  $\text{CO}_2$ , using an applied voltage of  $+0.1\text{ V}$  and UV-vis irradiation. The results were compared with photocatalytic reduction (using  $\text{Ti}/\text{TiO}_2\text{NT-ZIF-8}$  in  $0.1\text{ mol L}^{-1}$

$\text{Na}_2\text{SO}_4$  (pH 4.5), with UV-vis irradiation), photolytic reduction (in  $0.1\text{ mol L}^{-1}\text{ Na}_2\text{SO}_4$  (pH 4.5), with UV-vis irradiation), and electrochemical reduction (using  $\text{Ti}/\text{TiO}_2\text{NT-ZIF-8}$  in  $0.1\text{ mol L}^{-1}\text{ Na}_2\text{SO}_4$  (pH 4.5), with an applied voltage of  $+0.1\text{ V}$ ). The same tests were performed using  $\text{Ti}/\text{TiO}_2\text{NT}$  however, the concentration of all products found were below the quantification limit of the technique. The results are shown in Fig. 12.

The results obtained for the photolysis and electrolysis processes showed that there was no generation of any of the products analyzed during the three hours of treatment, demonstrating the importance of the  $\text{Ti}/\text{TiO}_2\text{NT-ZIF-8}$  catalyst in inducing the reduction.

For the PEC and PC processes revealed excellent performance of the former in the formation of methanol (Fig. 12A) and ethanol (B). The conversions of  $\text{CO}_2$  to methanol and ethanol using PEC were 75.8% and 52.7% higher, respectively, compared to use of PC. This suggested that in the reduction reactions, the bias potential reduced the effects of charge recombination by providing the photogenerated electrons

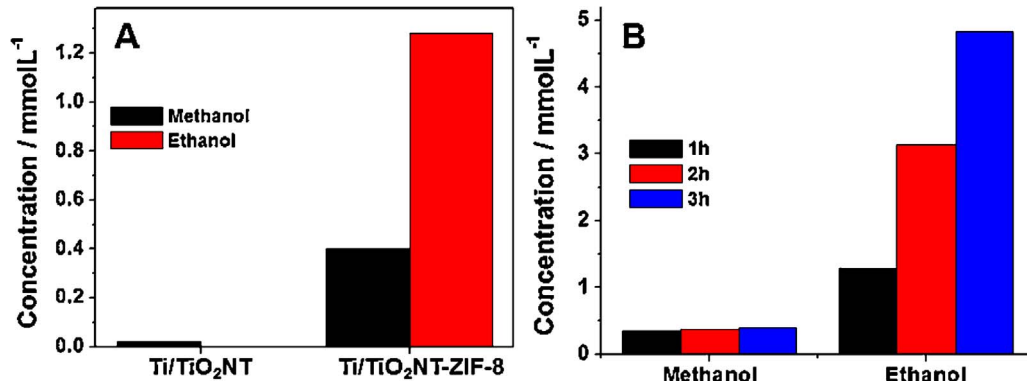
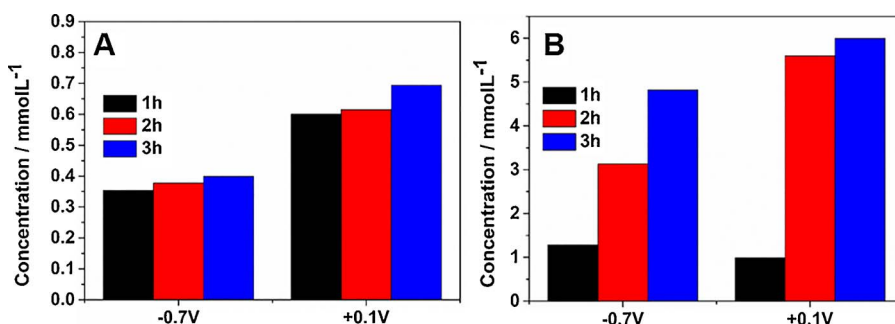


**Fig. 10.** Concentrations of methanol and ethanol generated in the photoelectrocatalytic processes at  $-0.7\text{ V}$  vs.  $\text{Ag}/\text{AgCl}$ , in  $0.1\text{ mol L}^{-1}\text{ Na}_2\text{SO}_4$  (pH 4.5), using (A) the  $\text{Ti}/\text{TiO}_2\text{NT}$  and  $\text{Ti}/\text{TiO}_2\text{NT-ZIF-8}$  electrodes for 1 h, and (B) the  $\text{Ti}/\text{TiO}_2\text{NT-ZIF-8}$  electrode for different times.



captured by the linker. These effects were also evaluated by Li et al. using ZIF-8 as a model compound for the evaluation of these deleterious effects in photocatalytic reactions, where a smaller recombination is observed in the presence of more thicker layers of this MOF [65]. The CO<sub>2</sub> preconcentrated in the form of carbamates enhanced the use of these available electrons by rapid electronic transfer, consequently increasing the concentrations of the photogenerated products. Specific faradaic efficiencies of 16% for methanol and 84% for ethanol were calculated at the end of three hours of PEC treatment. The separate electrolysis and photolysis processes did not lead to the generation of any products, even after 3 h of treatment.

The stability of the Ti/TiO<sub>2</sub>NT-ZIF-8 photoelectrode was determined comparing curves of the photocurrent vs potential obtained after a series of experiments over 50 h. The values showed differences that did not exceed 20 ± 2%. SEM images and IR spectrum of the electrode after 50 h of use are shown in Fig. S6 and Fig. S7. As can be observed, there was a significant decrease in the intensity of the CO<sub>2</sub> bands (at 2338 and 2359 cm<sup>-1</sup>) as well the appearance of an intense band at 1727 cm<sup>-1</sup> and a negative peak centered at 3330 cm<sup>-1</sup>, assigned to νC=O and νN–H of the carbamate species, respectively [66]. This behavior suggest that carbamate species are still be formed on the electrode surface in the presence of CO<sub>2</sub>.

As shown in the representative process provided in Scheme 1, the photoelectrochemical reductions of CO<sub>2</sub> to methanol and ethanol differed slightly and involved the reduction of carbamates formed on the Ti/TiO<sub>2</sub>NT-ZIF-8 electrode. The method was highly successful in transferring electrons generated from photoactivation by UV-vis light and an applied potential, able to reduce subsequently the carbamate to ethanol as a major product after transfer of 12 electrons and 12 protons. The presence of ZIF-8 nanoparticles on TiO<sub>2</sub> nanotubes provided a significant reduction in the band gap values of this material with a change in the potential of the conduction band making it more thermodynamically favorable the conversion of CO<sub>2</sub> to the photogenerated products.

In agreement with literature [67] and our findings the Scheme 1 resumes the CO<sub>2</sub> reduction mechanism at Ti/TiO<sub>2</sub>NT-ZIF-8 electrode illuminated by UV-vis light and under +0.1 V. The photoactivation of the electrode firstly produced highly reactive imidazole radicals [18,19], which interacted with the CO<sub>2</sub> present in solution, leading to the formation of carbamate compounds after preconcentration of the

Fig. 11. Concentrations of methanol (A) and ethanol (B) generated in the photoelectrocatalytic processes with bias potentials of -0.7 V and +0.1 V vs. Ag/AgCl, in 0.1 mol L<sup>-1</sup> Na<sub>2</sub>SO<sub>4</sub> (pH 4.5), using Ti/TiO<sub>2</sub>NT-ZIF-8 electrodes for 3 h.

dissolved gases on the surface of the Ti/TiO<sub>2</sub>NT-ZIF-8 electrode. These reactions occurred intensively throughout the experiment, with the electrons generated being attracted to the surfaces of the ZIF-8 nanoparticles and promoting the reduction to form methanol and ethanol in measurable concentrations. Our results indicate that the presence of nitrogenous groups in the ZIF-8 seems to be fundamental to selectively promote the reduction of CO<sub>2</sub> to methanol [67,68]. Thus, the first reduction step could be the pre-protonation of carbamate via H<sup>+</sup> abstraction and formic acid formation (Scheme 1). From the positioning of the calculated energy bands (Fig. S5), it is clear that the ZIF-8 coating Ti/TiO<sub>2</sub> increases the conduction band to higher energy levels, which can be favored with a slight advantage on conversion of CO<sub>2</sub>/ethanol due to the lower potential needed to promote the conversion from CO<sub>2</sub> [68]. But, probably the mechanism involves formation of formic acid, formaldehyde as unstable intermediate in the process and culminates in the formation of methanol and ethanol as main products. Our results corroborate with the formation of carbamates after the interaction of CO<sub>2</sub> dissolved in solution with the imidazoles groups of ZIF-8 favors the reduction to methanol as highlighted by Seshadri et al. [69] at overpotentials of only 0.2 V. According to these authors, this reaction occurs almost directly to methanol with very low concentrations of formic acid being formed during the reaction. The electron flow in the photoelectrocatalysis certainly is higher and the product reaches new reductive species such ethanol.

#### 4. Conclusions

A MOF-based hybrid chemical system was produced by growing nanoparticles on Ti/TiO<sub>2</sub>NT and was used as a photoelectrocatalyst for CO<sub>2</sub> reduction reactions in aqueous solution. FTIR spectroscopy analyses showed that host-guest interactions depended on the pore structure as well as the chemical nature of the MOF linker. The composite was constructed by the deposition of ZIF-8 nanoparticles on TiO<sub>2</sub> nanotubes and provided efficient photoelectrocatalytic conversion of CO<sub>2</sub> into methanol and ethanol fuels. The zinc-based MOF therefore acted not only in CO<sub>2</sub> adsorption/activation, but also as a co-catalyst, since it transferred the excited electrons for the photoelectrocatalytic reduction. We believe that the findings of this study constitute an important contribution to research on promising MOF-based catalysts for CO<sub>2</sub> photoelectroconversion, particularly concerning the interactions

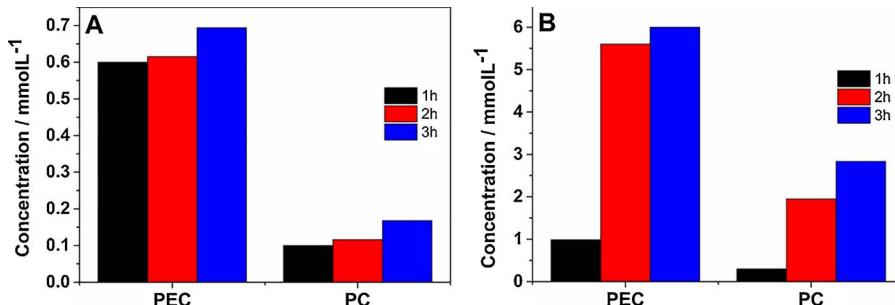


Fig. 12. Formation of methanol (A) and ethanol (B) using different techniques. Conditions: PEC (Ti/TiO<sub>2</sub>NT-ZIF-8 in 0.1 mol L<sup>-1</sup> Na<sub>2</sub>SO<sub>4</sub> (pH 4.5), E = +0.1 V, UV-vis irradiation); PC (Ti/TiO<sub>2</sub>NT-ZIF-8 in 0.1 mol L<sup>-1</sup> Na<sub>2</sub>SO<sub>4</sub> (pH 4.5), UV-vis irradiation). Illumination using a 125 W high pressure Hg vapor lamp.

between semiconductors and MOFs. It was very important to conclude that this is the first report on photoelectroreduction of CO<sub>2</sub> using MOFs as catalyst. In addition, a new perspective for researchers is opening, because of the real possibility to convert the more important greenhouse gas and very stable carbon dioxide into fuels through photoelectrocatalytic processes.

## Acknowledgements

The authors are grateful for the financial support provided by the Brazilian funding agencies FAPESP (#2015/18109-4 and #2014/50945-1 INCT-DATREM), CNPq (#152274/2016-2, #465571/2014-0, and #446245/2014-3), and CAPES. We are also indebted to GFQM-IQ for the X-ray diffraction measurements.

## Appendix A. Supplementary data

Supplementary data associated with this article can be found, in the online version, at <https://doi.org/10.1016/j.apcatb.2017.12.013>.

## References

- [1] A. Goeppert, G.K.S. Prakash, G.A. Olah, Recycling of carbon dioxide to methanol and derived products – closing the loop, *Chem. Soc. Rev.* 43 (2014) 7995–8048, <http://dx.doi.org/10.1039/C4CS00122B>.
- [2] S. Mozia, Generation of useful hydrocarbons and hydrogen during photocatalytic decomposition of acetic acid on CuO/rutile photocatalysts, *Int. J. Photoenergy* 2009 (2009) 1–8, <http://dx.doi.org/10.1155/2009/469069>.
- [3] L. Liu, Y. Li, Understanding the reaction mechanism of photocatalytic reduction of CO<sub>2</sub> with H<sub>2</sub>O on TiO<sub>2</sub>-based photocatalysts: a review, *Aerosol Air Qual. Res.* 14 (2014) 453–469, <http://dx.doi.org/10.4209/aaqr.2013.06.0186>.
- [4] X. Chen, S.S. Mao, Titanium dioxide nanomaterials: synthesis, properties, modifications, and applications, *Chem. Rev.* 107 (2007) 2891–2959, <http://dx.doi.org/10.1021/cr0500535>.
- [5] B. Chen, Z. Yang, Y. Zhu, Y. Xia, Zeolitic imidazolate framework materials: recent progress in synthesis and applications, *J. Mater. Chem. A* 2 (2014) 16811–16831, <http://dx.doi.org/10.1039/C4TA02984D>.
- [6] F.X.L. Xamena, J. Gascon, Metal Organic Frameworks as Heterogeneous Catalysts 12 RSC Catalysis Series, 2013, <http://dx.doi.org/10.1039/9781849734905>.
- [7] S.R. Batten, N.R. Champness, X.-M. Chen, J. Garcia-Martinez, S. Kitagawa, L. Öhrström, M. O'Keeffe, M.P. Suh, J. Reedijk, Coordination polymers, metal-organic frameworks and the need for terminology guidelines, *CrystEngComm* 14 (2012) 3001, <http://dx.doi.org/10.1039/c2ce06488j>.
- [8] H. Furukawa, K.E. Cordova, M.O. Keeffe, O.M. Yaghi, The chemistry and applications of metal-organic frameworks, *Science* 341 (2013) 1230444, <http://dx.doi.org/10.1126/science>.
- [9] H. Li, M. Eddaoudi, M. O'Keeffe, O.M. Yaghi, Design and synthesis of an exceptionally stable and highly porous metal-organic framework, *Nature* 402 (1999) 276–279, <http://dx.doi.org/10.1038/46248>.
- [10] K. Zhou, B. Mousavi, Z. Luo, S. Phatana Sri, S. Chaemchuen, F. Verpoort, Characterization and properties of Zn/Co zeolitic imidazolate frameworks vs. ZIF-8 and ZIF-67, *J. Mater. Chem. A* 0 (2016) 1–6, <http://dx.doi.org/10.1039/C6TA07860E>.
- [11] H.-P. Jing, C.-C. Wang, Y.-W. Zhang, P. Wang, R. Li, Photocatalytic degradation of methylene blue in ZIF-8, *RSC Adv.* 4 (2014) 54454–54462, <http://dx.doi.org/10.1039/C4RA08820D>.
- [12] J. Yao, H. Wang, Zeolitic imidazolate framework composite membranes and thin films: synthesis and applications, *Chem. Soc. Rev.* 43 (2014) 4470–4493, <http://dx.doi.org/10.1039/c3cs60480b>.
- [13] J.C. Cardoso, M.V. Boldrin Zanoni, M.V.B. Zanoni, Structural effects of nanotubes, nanowires, and nanoporous Ti/TiO<sub>2</sub> electrodes on photoelectrocatalytic oxidation of 4,4'-oxydianiline, *Sep. Sci. Technol.* 45 (2010) 1628–1636, <http://dx.doi.org/10.1080/01496395.2010.487721>.
- [14] L. Kong, X. Zhang, Y. Liu, S. Li, H. Liu, J. Qiu, K. Lun, In situ fabrication of high-permeance ZIF-8 tubular membranes in a continuous flow system, *Mater. Chem. Phys.* 148 (2014) 10–16, <http://dx.doi.org/10.1016/j.matchemphys.2014.07.036>.
- [15] T.M. McDonald, J.A. Mason, X. Kong, E.D. Bloch, D. Gygi, A. Dani, V. Crocella, F. Giordanino, S.O. Odoh, W.S. Drisdell, B. Vlaisavljevich, A.L. Dzubak, R. Poloni, S.K. Schnell, N. Planas, K. Lee, T. Pascal, L.F. Wan, D. Prendergast, J.B. Neaton, Cooperative insertion of CO<sub>2</sub> in diamine- appended metal-organic frameworks, *Nature* 519 (2015) 303–308, <http://dx.doi.org/10.1038/nature14327>.
- [16] C. Knofel, C. Martin, V. Hornebecq, P.L. Llewellyn, Study of carbon dioxide adsorption on mesoporous aminopropylsilane-functionalized silica and titania combining microcalorimetry and in situ infrared spectroscopy, *J. Phys. Chem. C* 113 (2009) 21726–21734, <http://dx.doi.org/10.1021/jp907054h>.
- [17] W. Zhao, D. Yan, J. Xu, H. Chen, In situ enzymatic ascorbic acid production as electron donor for CdS quantum dots equipped TiO<sub>2</sub> nanotubes: a general and efficient approach for new photoelectrochemical immunoassay, *Anal. Chem.* 84 (2012) 10518–10521, <http://dx.doi.org/10.1021/ac3028799>.
- [18] H.C. Robert, D. Mcalpine, Michael Cocivera, Photooxidation and reduction of ascorbic acid studied by E.S.R., *Can. J. Chem.* 51 (1973) 1682–1686.
- [19] C.J. Rhodes, An electron spin resonance study of imidazole radical cations, *J. Chem. Soc. Perkin Trans. 2* (1990) 725–727, <http://dx.doi.org/10.1039/P29900000725>.
- [20] G. Lu, O.K. Farha, W. Zhang, F. Huo, J.T. Hupp, Engineering ZIF-8 thin films for hybrid MOF-based devices, *Adv. Mater.* 24 (2012) 3970–3974, <http://dx.doi.org/10.1002/adma.201202116>.
- [21] C. Montoro, E. García, S. Calero, M.A. Pérez-Fernández, A.L. López, E. Barea, J.A. Navarro, Functionalisation of MOF open metal sites with pendant amines for CO<sub>2</sub>, *J. Mater. Chem.* 22 (2012) 10155–10158, <http://dx.doi.org/10.1039/c2jm16770k>.
- [22] J.L.C. Rowsell, O.M. Yaghi, Metal-organic frameworks: a new class of porous materials, *Microporous Mesoporous Mat.* 73 (2004) 3–14, <http://dx.doi.org/10.1016/j.micromeso.2004.03.034>.
- [23] H. Furukawa, K.E. Cordova, M. O'Keeffe, O.M. Yaghi, H. Furukawa, K.E. Cordova, M.O. Keeffe, O.M. Yaghi, The chemistry and applications of metal-organic frameworks, *Science* 9 (2010) 1230444, <http://dx.doi.org/10.1126/science.1230444>.
- [24] C.A. Trickett, A. Helal, B.A. Al-Maythalony, Z.H. Yamani, K.E. Cordova, O.M. Yaghi, The chemistry of metal-organic frameworks for CO<sub>2</sub> capture, regeneration and conversion, *Nat. Rev. Mater.* 2 (2017) 17045, <http://dx.doi.org/10.1038/natrevmats.2017.45>.
- [25] G.G. Bessegato, J.C. Cardoso, B.F. Da Silva, M.V.B. Zanoni, Enhanced photoabsorption properties of composites of Ti/TiO<sub>2</sub> nanotubes decorated by Sb<sub>2</sub>S<sub>3</sub> and improvement of degradation of hair dye, *J. Photochem. Photobiol. A Chem.* 276 (2013) 96–103, <http://dx.doi.org/10.1016/j.jphotochem.2013.12.001>.
- [26] J.C. Cardoso, T.M. Lizier, M.V.B. Zanoni, Highly ordered TiO<sub>2</sub> nanotube arrays and photoelectrocatalytic oxidation of aromatic amine, *Appl. Catal. B Environ.* 99 (2010) 96–102, <http://dx.doi.org/10.1016/j.apcatb.2010.06.005>.
- [27] F.A. Sayão, J.B. da Silva Flor, R.C.G. Frem, S. Stulp, J.C. Cardoso, M.V.B. Zanoni, Nitrite reduction enhancement on semiconducting electrode decorated with copper (II) aspirinate complex, *Electrocatalysis* (2016) 1–9, <http://dx.doi.org/10.1007/s12678-016-0327-9>.
- [28] G.G. Bessegato, J.C. Cardoso, B.F. Da Silva, M.V.B. Zanoni, Enhanced photoabsorption properties of composites of Ti/TiO<sub>2</sub> nanotubes decorated by Sb<sub>2</sub>S<sub>3</sub> and improvement of degradation of hair dye, *J. Photochem. Photobiol. A Chem.* 276 (2014) 96–103, <http://dx.doi.org/10.1016/j.jphotochem.2013.12.001>.
- [29] S. Stulp, J.C. Cardoso, J.F. de Brito, J.B.S. Flor, R.C.G. Frem, F.A. Sayão, M.V.B. Zanoni, An artificial photosynthesis system based on Ti/TiO<sub>2</sub> coated with Cu (II) aspirinate complex for CO<sub>2</sub> reduction to methanol, *Electrocatalysis* 8 (2017) 279–287, <http://dx.doi.org/10.1007/s12678-017-0367-9>.
- [30] J.F. De Brito, M. Valnica, B. Zanoni, On the application of Ti/TiO<sub>2</sub>/CuO n-p junction semiconductor: a case study of electrolyte, temperature and potential influence on CO<sub>2</sub> reduction, *Chem. Eng. J.* (2016) 15–18, <http://dx.doi.org/10.1016/j.cej.2016.08.033>.
- [31] T.T. Guaraldo, J.F. de Brito, D. Wood, M.V.B. Zanoni, A new Si/TiO<sub>2</sub>/Pt p-n junction semiconductor to demonstrate photoelectrochemical CO<sub>2</sub> conversion, *Electrochim. Acta* 185 (2015) 117–124, <http://dx.doi.org/10.1016/j.electacta.2015.10.077>.
- [32] S. Xie, Q. Zhang, G. Liu, Y. Wang, Photocatalytic and photoelectrocatalytic reduction of CO<sub>2</sub> using heterogeneous catalysts with controlled nanostructures, *Chem. Commun.* 52 (2015) 35–59, <http://dx.doi.org/10.1039/C5CC07613G>.
- [33] G.G. Bessegato, T.T. Guaraldo, J.F. de Brito, M.F. Brugnera, M.V.B. Zanoni, Achievements and trends in photoelectrocatalysis: from environmental to energy applications, *Electrocatalysis* 6 (2015) 415–441, <http://dx.doi.org/10.1007/s12678-015-0259-9>.
- [34] T.T. Guaraldo, J.F. de Brito, D. Wood, M.V.B. Zanoni, A new Si/TiO<sub>2</sub>/Pt p-n junction semiconductor to demonstrate photoelectrochemical CO<sub>2</sub> conversion, *Electrochim. Acta* 185 (2015) 117–124, <http://dx.doi.org/10.1016/j.electacta.2015.10.077>.
- [35] J.F. de Brito, A.R. Araujo, K. Rajeshwar, M.V.B. Zanoni, B. Zanoni, Photoelectrochemical reduction of CO<sub>2</sub> on Cu/Cu<sub>2</sub>O films: product distribution and pH effects, *Chem. Eng. J.* 264 (2015) 302–309, <http://dx.doi.org/10.1016/j.cej.2014.11.081>.
- [36] J.F. Brito, A.A. Silva, A.J. Cavalheiro, M.V.B. Zanoni, Evaluation of the parameters affecting the photoelectrocatalytic reduction of CO<sub>2</sub> to CH<sub>3</sub>OH at Cu/Cu<sub>2</sub>O electrode, *Int. J. Electrochem. Sci.* 9 (2014) 5961–5973.
- [37] B. Rungtaeworarat, J. Baek, J.R. Araujo, B.S. Archanjo, K.M. Choi, O.M. Yaghi, G.A. Somorjai, Copper nanocrystals encapsulated in Zr-based metal-organic frameworks for highly selective CO<sub>2</sub> hydrogenation to methanol, *Nano Lett.* 16 (2016) 7645–7649, <http://dx.doi.org/10.1021/acs.nanolett.6b03637>.
- [38] P.Z. Li, X.J. Wang, J. Liu, J.S. Lim, R. Zou, Y. Zhao, A triazole-containing metal-organic framework as a highly effective and substrate size-dependent catalyst for CO<sub>2</sub> conversion, *J. Am. Chem. Soc.* 138 (2016) 2142–2145, <http://dx.doi.org/10.1021/jacs.5b13335>.
- [39] R. Huang, Y. Peng, C. Wang, Z. Shi, W. Lin, A rhodium-functionalized metal-organic framework as a single-site catalyst for photochemical reduction of carbon dioxide, *Eur. J. Inorg. Chem.* 2016 (2016) 4358–4362, <http://dx.doi.org/10.1002/ejic.201600064>.
- [40] H. Zhang, T. Wang, J. Wang, H. Liu, T.D. Dao, M. Li, G. Liu, X. Meng, K. Chang, L. Shi, T. Nagao, J. Ye, Surface-plasmon-enhanced photodriven CO<sub>2</sub> reduction catalyzed by metal-organic-framework-derived iron nanoparticles encapsulated by ultrathin carbon layers, *Adv. Mater.* 28 (2016) 3703–3710, <http://dx.doi.org/10.1002/adma.201505187>.
- [41] C.-W. Kung, C.O. Audu, A.W. Peters, H. Noh, O.K. Farha, J.T. Hupp, Copper nanoparticles installed in metal-organic framework thin films are electrocatalytically competent for CO<sub>2</sub> reduction, *ACS Energy Lett.* (2017) 2394–2401, <http://dx.doi.org/10.1021/acsenergylett.7b00030>.

org/10.1021/acsenergylett.7b00621.

[42] I. Hod, M.D. Sampson, P. Deria, C.P. Kubiak, O.K. Farha, J.T. Hupp, Fe-porphyrin-based metal-organic framework films as high-surface concentration, heterogeneous catalysts for electrochemical reduction of CO<sub>2</sub>, *ACS Catal.* 5 (2015) 6302–6309, <http://dx.doi.org/10.1021/acscatal.5b01767>.

[43] N. Kornienko, Y. Zhao, C.S. Kley, C. Zhu, D. Kim, S. Lin, C.J. Chang, O.M. Yaghi, P. Yang, Metal-organic frameworks for electrocatalytic reduction of carbon dioxide, *J. Am. Chem. Soc.* 137 (2015) 14129–14135, <http://dx.doi.org/10.1021/jacs.5b08212>.

[44] I. Hod, O.K. Farha, J.T. Hupp, Electrocatalysis powered by porphyrin packing, *Nat. Mater.* 14 (2015) 1192–1193, <http://dx.doi.org/10.1038/nmat4494>.

[45] J.C. Cardoso, M.V. Boldrin Zanoni, Structural effects of nanotubes, nanowires, and nanoporous Ti/TiO<sub>2</sub> electrodes on photoelectrocatalytic oxidation of 4, 4-oxydianiline, *Sep. Sci. Technol.* 45 (2010) 1628–1636, <http://dx.doi.org/10.1080/01496395.2010.487721>.

[46] F. Tian, A.M. Cerro, A.M. Mosier, H.K. Wayment-Steele, R.S. Shine, A. Park, E.R. Webster, L.E. Johnson, M.S. Johal, L. Benz, Surface and stability characterization of a nanoporous ZIF-8 thin film, *J. Phys. Chem. C* 118 (2014) 14449–14456, <http://dx.doi.org/10.1021/jp5041053>.

[47] H. Chen, L. Wang, J. Yang, R.T. Yang, Investigation on hydrogenation of metal-organic frameworks HKUST-1, MIL-53, and ZIF-8 by hydrogen spillover, *J. Phys. Chem. C* 117 (2013) 7565–7576, <http://dx.doi.org/10.1021/jp401367k>.

[48] S. Liu, F. Chen, S. Li, X. Peng, Y. Xiong, Enhanced photocatalytic conversion of greenhouse gas CO<sub>2</sub> into solar fuels over g-C<sub>3</sub>N<sub>4</sub> nanotubes with decorated transparent ZIF-8 nanoclusters, *Appl. Catal. B Environ.* 211 (2017) 1–10, <http://dx.doi.org/10.1016/j.apcatb.2017.04.009>.

[49] G. Herzberg, *Molecular spectra and molecular structure, 18th ed.*, Infrared and Raman Spectra of Polyatomic Molecules Vol. 2 Krieger Pub Co, Princeton, 1945.

[50] A. Demessence, C. Boissière, D. Gross, P. Horcajada, C. Serre, G. Férey, G.J.a.a. Soler-Illia, C. Sanchez, Adsorption properties in high optical quality nanoZIF-8 thin films with tunable thickness, *J. Mater. Chem.* 20 (2010) 7676, <http://dx.doi.org/10.1039/c0jm00500b>.

[51] C.F. Windisch, P.K. Thallapally, B.P. McGrail, Adsorption of CO<sub>2</sub> on CoII<sub>3</sub>[CoII(CN)<sub>6</sub>]<sub>2</sub> using DRIFTS, *Spectrochim. Acta Part A Mol. Biomol. Spectrosc.* 74 (2009) 629–634, <http://dx.doi.org/10.1016/j.saa.2009.07.004>.

[52] Z. Hu, L. Zhang, J. Jiang, Development of a force field for zeolitic imidazolate framework-8 with structural flexibility, *J. Chem. Phys.* 136 (2012), <http://dx.doi.org/10.1063/1.4729314>.

[53] Y. Hu, Z. Liu, J. Xu, Y. Huang, Y. Song, Evidence of pressure enhanced CO<sub>2</sub> storage in ZIF-8 probed by FTIR spectroscopy, *J. Am. Chem. Soc.* 135 (2013) 9287–9290, <http://dx.doi.org/10.1021/ja403635b>.

[54] W.R. Lee, H. Jo, L.-M. Yang, H. Lee, D.W. Ryu, K.S. Lim, J.H. Song, D.Y. Min, S.S. Han, J.G. Seo, Y.K. Park, D. Moon, C.S. Hong, Exceptional CO<sub>2</sub> working capacity in a heterodiamine-grafted metal-organic framework, *Chem. Sci.* 6 (2015) 3697–3705, <http://dx.doi.org/10.1039/C5SC01191D>.

[55] T.M. McDonald, J.A. Mason, X. Kong, E.D. Bloch, D. Gygi, A. Dani, V. Crocellà, F. Giordanino, S.O. Odoh, W.S. Drisdell, B. Vlaisavljevich, A.L. Dzubak, R. Poloni, S.K. Schnell, N. Planas, K. Lee, T. Pascal, L.F. Wan, D. Prendergast, J.B. Neaton, B. Smit, J.B. Kortright, L. Gagliardi, S. Bordiga, A.J. Reimer, J.R. Long, Cooperative insertion of CO<sub>2</sub> in diamine-appended metal-organic frameworks, *Nature* 519 (2015) 303–308, <http://dx.doi.org/10.1038/nature14327>.

[56] M. Wang, J. Ioccozia, L. Sun, C. Lin, Z. Linb, Inorganic-modified semiconductor TiO<sub>2</sub> nanotube arrays for photocatalysis, *Energy Environ. Sci.* 4 (2014) 1–23, <http://dx.doi.org/10.1039/b000000x>.

[57] G.G. Bessegato, T.T. Guaraldo, M.V.B. Zanoni, Enhancement of photoelectrocatalysis efficiency by using nanostructured electrodes, in: M. Aliofkhazraei (Ed.), *Mod. Electrochem. Methods Nano, Surf. Corros. Sci.* InTech, 2014, pp. 271–319, <http://dx.doi.org/10.5772/57202>.

[58] J.C. Cardoso, N. Lucchiari, M.V.B. Zanoni, Bubble annular photoelectrocatalytic reactor with TiO<sub>2</sub> nanotubes arrays applied in the textile wastewater, *J. Environ. Chem. Eng.* 3 (2015) 1177–1184, <http://dx.doi.org/10.1016/j.jece.2015.04.010>.

[59] J.C. Cardoso, G.G. Bessegato, M.V.B. Zanoni, Efficiency comparison of ozonation, photolysis, photocatalysis and photoelectrocatalysis methods in real textile wastewater decolorization, *Water Res.* 98 (2016) 39–46, <http://dx.doi.org/10.1016/j.watres.2016.04.004>.

[60] A. Molinari, L. Samiolo, R. Amadelli, EPR spin trapping evidence of radical intermediates in the photo-reduction of bicarbonate/CO<sub>2</sub> in TiO<sub>2</sub> aqueous suspensions, *Photochem. Photobiol. Sci.* (2015) 1039–1046, <http://dx.doi.org/10.1039/C4PP00467A>.

[61] A. Vimont, A. Travert, P. Bazin, J. Lavalley, M. Daturi, C. Serre, Evidence of CO<sub>2</sub> molecule acting as an electron acceptor on a nanoporous metal-organic-framework MIL-53 or Cr<sup>3+</sup>(OH)(O<sub>2</sub>C-C<sub>6</sub>H<sub>4</sub>-CO<sub>2</sub>), *Chem. Commun.* 0 (2007) 3291–3293, <http://dx.doi.org/10.1039/b703468g>.

[62] J. Hong, W. Zhang, J. Ren, R. Xu, Photocatalytic reduction of CO<sub>2</sub>: a brief review on product analysis and systematic methods, *Anal. Methods* 5 (2013) 1086–1097, <http://dx.doi.org/10.1039/c0xx00000x>.

[63] K. Bhattacharyya, A. Danon, B.K. Vijayan, K.a. Gray, P.C. Stair, E. Weitz, Role of the surface Lewis acid and base sites in the adsorption of CO<sub>2</sub> on titania nanotubes and platinized titania nanotubes: an in situ FT-IR study, *J. Phys. Chem. C* 117 (2013) 12661–12678, <http://dx.doi.org/10.1021/jp402979m>.

[64] G.G. Bessegato, F.F. Hudari, M.V.B. Zanoni, Self-doped TiO<sub>2</sub> nanotube electrodes: a powerful tool as a sensor platform for electroanalytical applications, *Electrochim. Acta* 235 (2017) 527–533, <http://dx.doi.org/10.1016/j.electacta.2017.03.141>.

[65] Y. Li, A. Pang, C. Wang, M. Wei, Metal-organic frameworks: promising materials for improving the open circuit voltage of dye-sensitized solar cells, *J. Mater. Chem.* 21 (2011) 17259, <http://dx.doi.org/10.1039/c1jm12754c>.

[66] P.C. Danon, FTIR study of CO<sub>2</sub> adsorption on amine-grafted SBA-15: elucidation of adsorbed species, *J. Phys. Chem.* 115 (2011) 11540–11549.

[67] A.J. Morris, R.T. McGibbon, A.B. Bocarsly, Electrocatalytic carbon dioxide activation: the rate-determining step of pyridinium-catalyzed CO<sub>2</sub> reduction, *ChemSusChem* 4 (2011) 191–196, <http://dx.doi.org/10.1002/cssc.201000379>.

[68] C. Finn, S. Schnittger, L.J. Yellowlees, Molecular approaches to the electrochemical reduction of carbon dioxide, *Chem. Commun.* 48 (2012) 1392–1399, <http://dx.doi.org/10.1039/C1CC15393E>.

[69] G. Seshadri, C. Lin, A.B. Bocarsly, A new homogeneous electrocatalyst for the reduction of carbon dioxide to methanol at low overpotential, *J. Electroanal. Chem.* 372 (1994) 145–150, [http://dx.doi.org/10.1016/0022-0728\(94\)03300-5](http://dx.doi.org/10.1016/0022-0728(94)03300-5).